On the shear thinning of non-Brownian suspensions: friction or adhesion?

Anastasia Papadopoulou[1,2], Jurriaan J. Gillissen[3], Helen J. Wilson[3], Manish K. Tiwari[2,4], Stavroula Balabani[1]*

[1]*FLUME, Department of Mechanical Engineering, University College London, Torrington Place, London, WC1E 7JE, UK*

[2]*Nanoengineered Systems Laboratory, Department of Mechanical Engineering, University College London, Torrington Place, London, WC1E 7JE, UK*

[3]*Department of Mathematics, University College London, London, Gower Street, London WC1E 6BT, UK*

[4]*Wellcome/EPSRC Centre for Interventional and Surgical Sciences (WEISS), University College London, W1W 7TS, UK*

** Corresponding author: s.balabani@ucl.ac.uk*

Abstract

Shear thinning is fundamental to a broad range of particle suspensions, both in nature and in industrial applications. Yet the mechanisms governing it remain unclear. In particular, the distinct, and often competing, roles of the interparticle, particle-fluid interactions and the particle surface morphology need clarity. By using non-Brownian silica particles with different morphology, surface functional groups and suspending media, here we reveal two different shear thinning mechanisms, controlled either by frictional or adhesion forces between particles. Smooth glass sphere suspensions in a polar medium (glycerol), where particles interact strongly with the solvent, showed no shear thinning even at high volume fractions ($\varphi \geq 0.5$), while rough silica particles, with similar size distribution, induced shear thinning behaviour at φ values of 0.25 and above. The latter is attributed to the increased frictional contacts in rough and irregular particles. Considering surface irregularity as elastically deformable asperities enabled us to estimate the critical load above which two neighbouring rough particles experience frictional contacts giving rise to shear thinning. In contrast, in a non-polar (mineral oil) solvent, with which the particles do not interact strongly, both glass spheres and the rough silicas showed a pronounced shear thinning response and yield stress behaviour at volume fractions as low as 2% v/v. The rheology of these suspensions is dictated by the adhesion forces between the particles that lead to the formation of large agglomerates, which breakdown under increasing shear. The evolution of the sheared suspensions microstructure was captured using an optical shearing cell, which also enabled us to quantify the particle agglomeration characteristics using an aggregation index. To demonstrate the generality of our approach, we modified the surface chemistry of the glass spheres by introducing hydrophobic groups (e.g. a fluorosilane or palmitic acid) to inhibit inter-particle interactions and improve the dispersion of the otherwise inherently hydrophilic glass spheres in mineral oil; as expected, this suppressed the shear thinning behaviour of the suspensions. The present results clearly elucidate alternative design routes to controlling suspension rheology, whether to promote or suppress shear thinning, offering new insights for the manufacturing and manipulation of complex particle suspensions.

Key words: silica particles, suspension rheology, frictional contacts, adhesion, microstructure, hydrophobicity.

1. Introduction

Particle suspension rheology is of significant importance in numerous industrial and natural applications and has been the focus of extensive research. Particle suspensions exhibit a wide range of rheological phenomena as a function of applied shear rate and concentration. Shear thinning, i.e. a decrease in the viscosity values with increasing shear rate, is a typical non-Newtonian behaviour of suspensions, attributed to interparticle and particle-fluid interactions as well as changes in the microstructure under shear.

Four main mechanisms have been proposed in the literature so far to explain the origin of shear thinning suspension rheology; namely particle structuring under shear, shear thinning of interparticle gap fluids, frictional and adhesive interparticle interactions. Gadala-Maria and Acrivos (1980) were among the first to explore the mechanism behind shear thinning through studying the rheology of highly concentrated (φ≥0.3) non-Brownian polystyrene spheres (40-50 μm) in a mixture of silicone oils. The shear thinning behaviour of these suspensions was attributed to an anisotropic structuring of the particles under shear. In a more recent study, Vàzquez-Quesada et al. (2016) used a numerical approach and showed that the shear thinning of non-colloidal particles in a macroscopically Newtonian fluid (silicone oil) stems from the shear thinning behaviour of the suspending medium at extremely high shear stresses experienced within the interparticle gaps. This is understandable considering that silicone oils consist of polymer chains with various lengths, which align in the direction of flow at sufficiently high shear rates, inducing thus a shear thinning response.

More recent research eluded a very strong role played by interparticle interactions in determining shear thinning behaviour. More specifically, shear thinning was found to be dominated by frictional contacts between the particles at sufficiently high normal loads, as evidenced by the experiments of Chatté et al. (2018) with smooth polyvinyl chloride (PVC) particles with few asperities in a Newtonian plasticizer. Considering the surface irregularities as elastically deformable and based on the theory of Archard (1957) for the elastic deformation of rough surfaces, they were able to demonstrate that shear thinning stems from a reduced microscopic friction coefficient between particles as the asperities deform during contact. Lobry et al. (2019) further supported this shear thinning mechanism by studying the rheology of relatively smooth polystyrene (PS) particles in silicone oil.

Blanc et al. (2018) provided additional evidence in support of the theory introduced by Chatté et al. (2018). In their study, the rheology of relatively smooth and monodisperse polystyrene spheres ($d{\sim}80\mu m$) and irregularly shaped (faceted) sugar particles ($d{\sim}80-100\mu m$) in a Newtonian silicone oil matrix was investigated. Irregularly shaped particles were shown to exhibit higher zero shear viscosities and pronounced shear thinning compared to the polystyrene spheres at the same particle volume fractions. The non-Newtonian rheology of the faceted particles was attributed to the higher contribution of the contact viscosity to the total viscosity value of the suspension at increasing particle volume fraction and decreasing applied shear stress; as particle

contacts are favoured in the case of irregularly shaped particles (Blanc et al., 2018; Gallier et al., 2014). In contrast, suspensions of relatively smooth spheres showed weak shear thinning response due to mild surface deformation (non-linear Hertz contact).

However, the physical properties of the solvent can also play a significant role to suspension rheology (Amiri et al., 2012; Saint-Michel et al., 2019). For instance, Amiri et al. (2012) studied the rheology of fumed silica suspensions in water/glycerol solutions. They observed that increasing the glycerol content in the suspending medium led to more stable suspensions, despite a decrease in the z-potential. This behaviour revealed the existence of a new stabilisation force, which was related to the formation of a solvation layer around the particles and the subsequent hindering of interparticle contacts. Similar behaviour was observed for non-Brownian glass spheres in an aqueous Newtonian solvent (Saint-Michel et al., 2019).

On the other hand, when particles are suspended in solvents which promote particle attraction, adhesion forces are expected to dominate suspension rheology. Therefore, in the presence of adhesive systems, the shear thinning rheology is governed by the formation of agglomerates which break down under increasing applied deformations. This leads to the large structures reducing to smaller units and thus, lowering the viscosity values with increasing shear rate, as has been demonstrated in biological fluids such as blood as well as silica particle suspensions (Eberle et al., 2014; Kaliviotis and Yianneskis, 2007; Min Kim et al., 2014). Thus, the shear induced microstructural changes of suspensions of adhesive particles play a key role in the shear thinning of such particle systems; these are also highly dependent on particle size distribution, volume fraction and surface characteristics (Blanc et al., 2018; Mewis and Wagner, 2012). For example**,** when Brownian motion is significant, due to the presence of small, submicron particles, agglomeration is favoured by the larger available surface for particle contacts leading to more pronounced shear thinning rheology (Mewis and Wagner, 2012).

Various methods have been employed to probe suspension microstructure, including simulations, spectroscopic techniques and oscillatory shear rheology (Egres et al., 2006; Gadala-Maria and Acrivos, 1980; Kalman and Wagner, 2009; Morris, 2009; Sierou and Brady, 2002). Visualisation of dense particle suspension microstructure is challenging and thus optical imaging and actual quantification of the shear-induced characteristics of such systems has been fairly limited; to date very few relevant studies exist mainly focusing on smooth or spherical particles and biological samples, such as blood (Gunes et al., 2008; Kaliviotis et al., 2016; Lin et al., 2018; Ma et al., 2008; Massaro et al., 2020; Tanner, 2015; Varga et al., 2019).

Despite the huge amount of research conducted on investigating the specific mechanisms governing shear thinning behaviour in particle suspensions (Gallier et al., 2014; Marunaka and Kawaguchi, 2014; Moon et al., 2015; Selimovic et al., 2007; Tanner, 2018), it still remains unclear how exactly particle surface morphology and surface functional groups as well as the physical properties of the solvent-carrier media influence particle interactions and thus rheology. Silica particles have been widely used as model systems in many studies (Chen et al., 2005; De Kruif et al., 1985; Galindo-Rosales and Rubio-Hernandez, 2009; Katepalli et al., 2017; Maranzano and

Wagner, 2001; Raghavan et al., 2000; Selimovic et al., 2007; Zhou et al., 1995) not only due to their high relevance to both industrial and natural applications, but also due to their unique properties of being eminently amenable to variations in morphology and surface chemistry.

The present study aims to probe the driving mechanisms that lead to the shear thinning behaviour of non-Brownian particle suspensions by tuning interparticle interactions in systems of smooth glass spheres and commercial silica particles. Three different routes to vary interparticle interactions will be utilised, namely particle surface roughness, surface chemistry and solvent physical properties, i.e. polar (glycerol) vs non-polar (mineral oil), in an attempt to reveal or suppress particle suspension shear thinning rheology and provide clear links with the mechanisms proposed above. Optical shearing methods will be applied to relatively dilute suspensions to visualise the shear induced structuring (i.e. local microstructure) of the particles *in situ* and further elucidate the observed bulk rheological phenomena. The suspension rheology will also be controlled through the introduction of hydrophobic groups on glass spheres and their dispersion properties in mineral oil will be evaluated. Our findings of bulk and local rheology are intended to provide a fundamental understanding of how silica particles with different surface morphologies and chemistry behave in diverse environments, offering thus, new insights in the manufacturing of complex formulations.

2. Materials and Methods

2.1 Particle suspensions

Commercial grade silica particles ($D = 17.5 \pm 15.2\ \mu m$), supplied in-kind by GSK and called silicas hereafter, and hollow glass spheres ($D = 11 \pm 5.5\ \mu m$) (Sigma Aldrich) were suspended in two Newtonian media; one polar, namely glycerol (≥99.5%), and the other non-polar, i.e. mineral oil (Sigma Aldrich). Table 1 summarizes the properties of the two particles and those of the suspending media. The size distribution of the particles was derived using laser diffraction, the surface morphology was evaluated through Scanning Electron Microscopy (SEM) and image analysis, whereas the specific surface area and porosity were calculated using the Brunauer-Emmet-Teller (BET) method. SEM micrographs and the corresponding size distributions of the two types of particles are shown in Figure 1. Commercial silicas consist of primary particles with diameter ~10 nm, which are fused together to irreducible aggregates of irregular shapes (Fig. 1b).

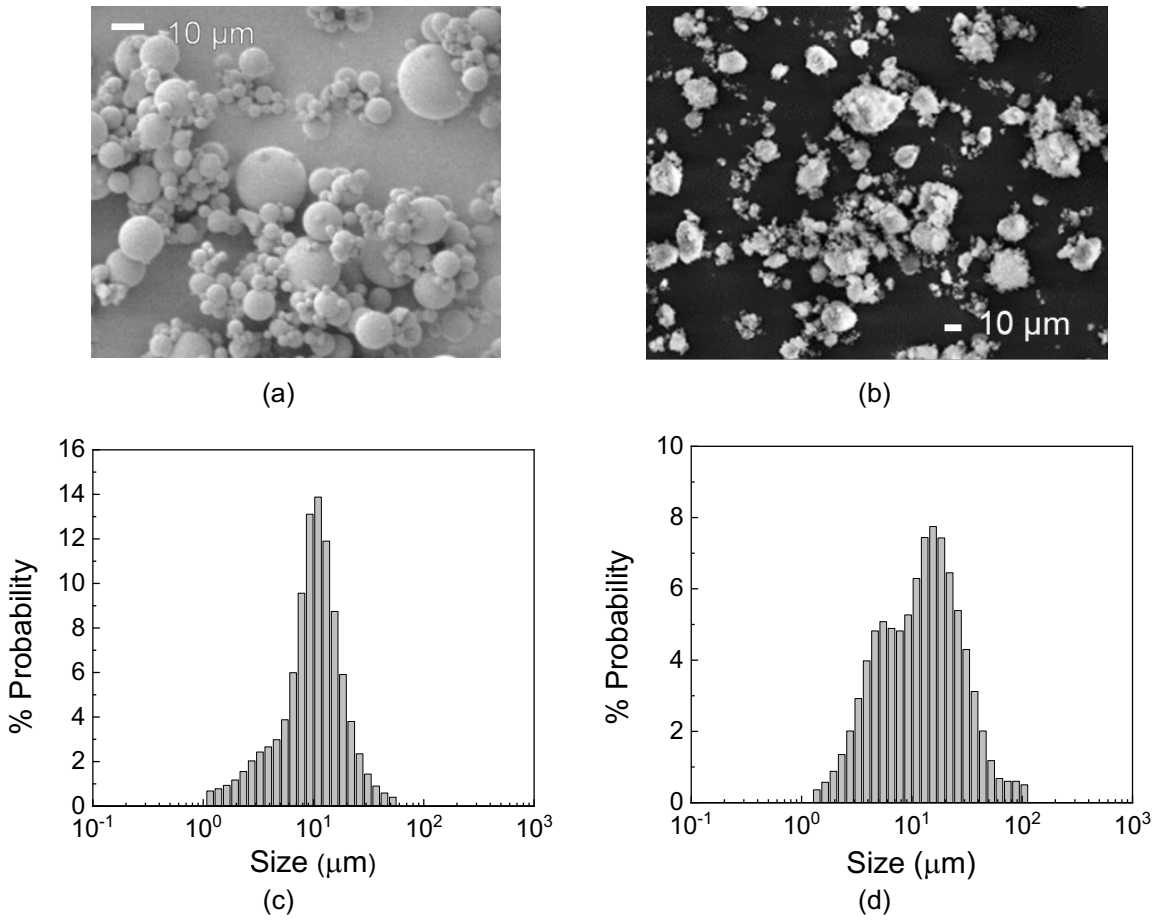

Figure 1. SEM micrographs and size distributions of a), c) glass spheres & b), d) aggregated silicas.

Table 1. Physical properties of the particles and the suspending media used in this study.

Particle properties	**Glass spheres**	**Silicas**
Density ($\rho_p,\ g/ml$)	1.1	2.0
Diameter (*D, µm*)	11±5.5	17.5 ±15.2
Specific surface area (*S, m^2/g*)[*1]	1.6	51.9
Porosity[*1]	-	68.5%
Fluid properties at 20°C	**Glycerol**	**Mineral oil**
Density ($\rho_f,\ g/ml$)	1.25	0.87
Viscosity ($\eta_f,\ Pa.s$)	1.3 ($\eta_{f,G}$)	0.03 ($\eta_{f,MO}$)

[*1]: obtained from the BET method.

2.2 Sample preparation

The required amount of particle mass to achieve a given volume fraction was dispersed in the suspending medium, i.e. glycerol or mineral oil, and mixed using a high shear mixer (Silverson, Model L5M). Mixing time varied from 5 to 10 minutes at a rotating speed between 3500 and 4000

rpm. Microscopic images of the suspensions after preparation showed that high shear mixing did not induce any particle breakage. Particle concentrations in glycerol were varied between 0-62% according to particle type and dispersion capacity, resulting in volume fractions (φ) ranging from 0 to 0.62. In the case of mineral oil, the maximum volume fraction used was $\varphi = 0.15$. The maximum φ for each suspension was based on visual observations to ensure that the mixture was homogeneous, and no clumps of undispersed powder were present and does not correspondent to the maximum packing fraction. Further increase of the particle concentration in each solvent led to inhomogeneities and the inability of evenly dispersing the solids into the solvent. Entrained air bubbles were removed under vacuum and the rheological measurements were conducted immediately after that stage to minimize particle sedimentation.

2.3 Particle surface chemistry modification

The surface chemistry of the glass spheres was modified using two different self-assembled monolayers, 1H,1H,2H,2H-Perfluorooctyltriethoxysilane and palmitic acid (Sigma Aldrich) to introduce hydrophobic groups on their surface. This enabled controlling interparticle interactions and improving particle dispersion in mineral oil. The treatment process was conducted as follows: solutions of the hydrophobic chemicals with specified concentrations were prepared in ethanol for the palmitic acid and in hexane for the fluorosilane and then the particles were added in different mass ratios in relation to the reagent. The suspensions were magnetically stirred for at least two hours to ensure good dispersion and sufficient contact time between the particles and the silane or the palmitic acid respectively. Finally, the particles were separated from the solvent by centrifugation and left to dry overnight.

2.4 Shear rheology

The rheological properties of the suspensions were measured using a hybrid stress controlled rotational rheometer (DHR-3, TA Instruments) using a sandblasted (R_a= 1.8−2 μm) parallel plate geometry with a diameter of 40 mm and an average gap of 650 μm, which is at least 30 times larger than the average particle diameter, was employed. All measurements were conducted at 20°C. The temperature of the lower plate was controlled using a Peltier system with an accuracy of ±0.1°C. A solvent evaporation trap was used to hinder sample evaporation during all measurements. The experimental procedure is explained below.

Particle suspensions are sensitive to shearing conditions and therefore, the samples were first pre-sheared at a constant shear rate of 200 s^{-1} for 300 s to ensure the same shear history, followed by a resting period of 300 s to allow sample equilibration (Khandavalli and Rothstein, 2015; Ma et al., 2017; Varga et al., 2019). Steady state flow sweeps were conducted at increasing shear rates ($\dot{\gamma}$) from 10^{-3} s^{-1} to 10^{3} s^{-1}. The presence of hysteretic loops under shear was evaluated by performing a subsequent steady state flow sweep with decreasing shear rate values in the same range. Samples were allowed to rest for 5 min between the flow sweeps. During the resting period,

non-destructive time sweeps, i.e. small amplitude oscillatory shear time sweeps at a strain amplitude of $\gamma = 0.1\%$ and frequency of $f = 1Hz$, were performed to monitor the evolution of the storage (G') and loss (G'') moduli and evaluate any possible particle sedimentation during the equilibration time. All measurements were conducted in triplicate to ensure repeatability of the results, while the stress, and corresponding viscosity values, were calculated using Eq. 1, to account for the non-uniform shear rate in the parallel plate geometry (Gamonpilas et al., 2016).

$$\tau_{true} = \frac{M}{2\pi R^3}\left(3 + \frac{dlnM}{dln\dot{\gamma}_R}\right) \quad (1)$$

where τ_{true} is the corrected shear stress (Pa), M is the measured torque (N.m), R is the radius of the measuring system (m) and $\dot{\gamma}_R$ is the maximum shear rate at the rim of the geometry (s^{-1}).

Due to the density mismatch between the particles and the suspending medium, especially in the case of mineral oil, the flow sweeps need be performed at sufficiently high stresses to avoid particle sedimentation. This critical stress is determined using the dimensionless Shields parameter, defined as the ratio of the fluid force acting on the particle to the particle weight (Lobry et al., 2019).

$$Sh = \frac{\tau}{2a\Delta\rho g} \quad (2)$$

where τ is the shear stress (Pa), a the particle radius (m), $\Delta\rho$ the particle-fluid density difference (kg/m^3) and g the gravitational acceleration (m/s^2). Therefore, only data at stresses higher than the limit of $Sh = 1$ (i.e. 0.01 Pa and 0.09 Pa for the glass spheres and silicas in glycerol, 0.14 Pa and 1.2 Pa for the corresponding suspensions in mineral oil) are presented.

The *Pèclet* number ($Pe = 6\pi\alpha^3\dot{\gamma}\eta_f/k_BT$, where α is the average particle radius) varied from $1.5{\cdot}10^4$ to $3.2{\cdot}10^9$ for suspensions in glycerol and from $3.5{\cdot}10^4$ to $7.4{\cdot}10^7$ for suspensions in glycerol and in mineral oil, respectively, in the shear rate range studied. It should be noted that although the estimated $Pè$ numbers are sufficiently large to assume that Brownian motion is negligible, the particles used in the present study are highly polydisperse with the smallest sizes falling into the colloidal regime, i.e. $d < 1\ \mu m$. Therefore, some Brownian motion is expected to influence the rheological response of the suspensions. To evaluate the extent of this effect we calculated the critical shear rate at which the percentage of particles capable of inducing Brownian effects is below 1%. based on the size distribution in Fig. 1 and $Pè = 10$ (Foss and Brady, 2000); the estimated shear rates were $\dot{\gamma} = 0.04\ s^{-1}$ for the glass spheres and $\dot{\gamma} = 0.004\ s^{-1}$ for the silicas. This indicates that Brownian motion effects are expected to have a minor influence on the acquired data for the highly concentrated suspensions only and a limited shear rate range. Suspensions in mineral showed severe sedimentation at low shear rates and thus, the shear rates presented for these suspensions are well above the estimated $\dot{\gamma}$ for Brownian motion to influence the results. Therefore, no Brownian effects are expected for the corresponding cases.

The shear thinning response of the concentrated suspensions of rough silicas in glycerol was described by the Carreau equation (Boyd et al., 2007).

$$\eta = \eta_\infty + (\eta_0 - \eta_\infty)(1 + (\lambda\dot{\gamma})^2)^{\frac{n-1}{2}} \quad (3)$$

where η_0 and η_∞ are the zero-shear rate and infinite-shear rate viscosities (Pa.s), λ is the relaxation time (s) and n is the flow index (n=1 corresponds to Newtonian fluids, while n<1 describes the shear thinning response) (Macosko, 1994).

The Herschel-Bulkley model was used to fit the viscosity data derived from the suspensions in mineral oil (Dinkgreve et al., 2016).

$$\eta = \eta_\infty + \frac{\tau_y}{\dot{\gamma}}(1 + (\lambda\dot{\gamma})^n) \quad (4)$$

where η_∞ is the suspensions viscosity at infinite shear rate (Pa.s), τ_y is the yield stress (Pa) and λ is the relaxation time (s). Eq. 4 implies that at small shear rates ($\dot{\gamma} \to 0$) the suspensions show dynamic yield stress behaviour, while at the high rate limit the viscosity thins down with a flow index n in order to reach an asymptotic infinite shear viscosity, η_∞.

The relative viscosity values as a function of particle volume fraction were well fitted with the Krieger-Dougherty model (Eq. 5) (Krieger and Dougherty, 1959).

$$\eta_r = \left(1 - \frac{\varphi}{\varphi_m}\right)^{-B\varphi_m} \quad (5)$$

where φ_m is the maximum packing fraction, B is the intrinsic viscosity. Alternative empirical models were also considered as detailed in Appendix A.

2.5 Optical shearing measurements

The microstructure of the suspensions was investigated by means of an optical shearing method. The experimental set up is depicted in Figure 2. The sample was placed between the two quartz plates of a Couette shearing cell (CSS-450, Linkam Scientific Ltd.) and pre-sheared at a constant shear rate of $\dot{\gamma} = 200\ s^{-1}$ for 5 min. Shearing was applied after a resting period of 5 mins at shear rates varying from 5 s^{-1} to 500 s^{-1} (i.e. 5 s^{-1}, 10 s^{-1}, 25 s^{-1}, 40 s^{-1}, 60 s^{-1}, 100 s^{-1}, 250 s^{-1}, 500 s^{-1}). The sample was kept at each shear rate for 1 or 2 mins before image acquisition. The above procedure was followed to mimic the bulk rheological measurements performed with the rheometer. All experiments were conducted using a gap of 100 μm, to minimise the effects of the out of plane particles and at room temperature (*ca* 25°C). The sheared suspensions were illuminated using a fiber optic LED (SugarCube Ultra, Edmund Optics) and images were acquired using a high-speed CMOS camera (IDT X3) attached on a microscope assembly. The latter was equipped with a 20x objective (NA: 0.6). On average, 2000 images were acquired for each case at frame rates varying from 30 Hz to 300 Hz, depending on the shear rate, and at a resolution of

1280x1024 px^2. The visualisation was made in the flow (velocity) plane and thus, shear banding effects in the depth (vorticity) direction could not be observed. The captured images were processed in MATLAB to extract an aggregation index, as described in Kaliviotis et al. (2016). The aggregation index (A) was employed to quantify particle agglomeration and/or disaggregation as a function of shear, defined as the ratio of the total particle free area, observed in the microscopy images, to the expected area covered by the suspending medium according to the particle volume fraction:

$$A = \frac{Total\ particle\ free\ area}{(1-\varphi)\ Total\ area}\ 100\% \tag{6}$$

Other indices were also estimated from the image analysis, such as the ratio of the total particle free area to the total area covered by the particles and the image intensity correlation factor. All indices showed similar trends with the aggregation index defined above and thus, only this index will be reported here.

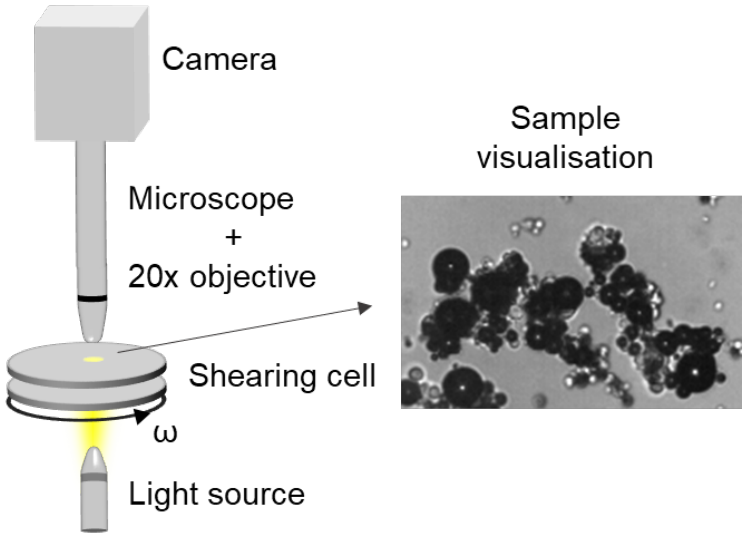

Figure 2. Experimental setup of the optical shearing technique. The system consists of an optical shearing cell, a microscope assembly, a high-speed camera and LED illumination.

3. Results and discussion

In the following sections the dramatically different nature of rheology and shear thinning property in silica particle suspensions with variations in particle surface morphology and suspending media will be firstly demonstrated through corresponding flow curves acquired at various volume fractions. By further analysing these data and coupling them with optical shearing measurements of suspension microstructure, the conditions for friction led and adhesive shear thinning are elucidated. This understanding is subsequently exploited to demonstrate rheology control through simple surface functionalisation.

3.1 Suspension rheology in glycerol-friction induced shear thinning

Both glycerol and silica are hydrophilic with copious amounts of hydroxyl groups (-OH). Although silica particles tend to attract themselves through the free hydroxyl groups on their surface, when suspended in a polar solvent containing hydroxyl groups, such as glycerol, a so-called solvation layer is formed around the particles which acts as a barrier to interparticle attraction. The thickness and strength of this solvation layer has been found to strongly depend on the percentage of water in glycerol as well as temperature as the latter affects glycerol viscosity (Amiri et al., 2012; Gao et al., 2017; Saint-Michel et al., 2019). Therefore, we would expect the rheology of both glass sphere and silica suspensions in glycerol to be strongly influenced by the particle-solvent interactions. In the following sections, the rheological properties of the suspensions will be discussed on the basis of both particle-particle and/or particle-solvent attraction.

The relative viscosity (η_r=η_s/η_f) and shear stress for all particle suspensions in glycerol are plotted in Figure 3 as a function of shear rate and particle volume fraction. A clear dependence of suspension rheology on the shear rate, particle volume fraction and surface roughness is revealed. In the range of concentrations studied, the ‘smooth’ glass spheres show almost no evidence of shear thinning, while mild shear thickening is observed for φ≥0.50. On the contrary, silicas exhibit a pronounced shear thinning response at the same volume fractions, especially for φ≥0.25, similar to that observed by Blanc et al. (2018) for faceted sugar particles suspended in a Newtonian silicone oil.

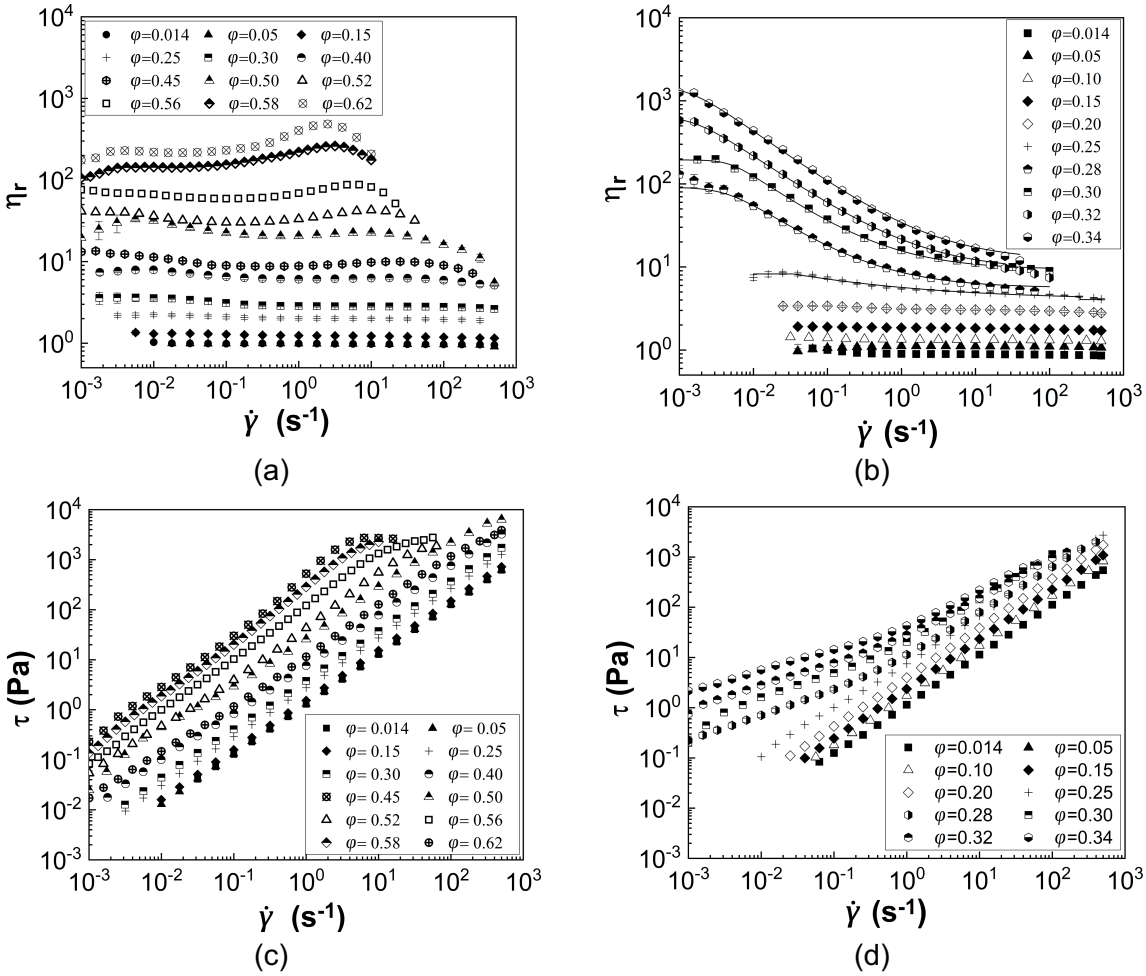

Figure 3. Steady state shear relative viscosity and shear stress of a), c) glass sphere and b), d) silica particle suspensions in glycerol at 20°C as a function of shear rate. Solid lines in (b) represent the Carreau equation fittings.

The above results should be interpreted in the light of strong interaction between particles (glass sphere or silica) with glycerol, which will dominate over inter-particle attraction (adhesion). Friction enabled thinning offers a plausible means to understand the results in Figure 3. The friction-driven theory employs the concept of a critical normal load to describe the non-Newtonian behaviour of suspensions of rough, non-Brownian particles (Archard, 1957; Chatté et al., 2018; Lobry et al., 2019). More specifically, Lobry et al. (2019) and Chattè et al. (2018) combined simulations with experiments, using non-Brownian PS particles in silicone oil and PVC particles in a plasticizer respectively. These studies showed that shear thinning in a few-asperities system stems from the elastic deformation of the surface asperities leading to a reduction in the friction coefficient, confirming the findings of Archard (1957). In other words, particle surface asperities are directly linked to modulation of friction between particles which leads to a shear thinning rheology.

In Fig. 3, it can be clearly seen that for smooth glass spheres, the lack of asperities along with the presence of a thick solvation layer formed from glycerol, limits interparticle contacts and results in significantly suppressing the shear thinning response. This is in contrast to the observations of Saint-Michel et al. (2019) who reported considerable shear thinning of glass

sphere suspensions in an aqueous solution. However, in the presence of water higher interparticle interactions are expected due to the much lower viscosity of the solvent and the fact that water molecules have only one hydroxyl group (-OH) to bind on silicas, compared to glycerol which has three. On the other hand, at very high particle loading, where glycerol concentration is low resulting in thin solvation layers susceptible to shearing conditions, long range, jamming networks are likely to occur, i.e. at $\varphi > 0.50$, leading to shear thickening.

Unlike glass sphere suspensions, silicas showed pronounced shear thinning at $\varphi \geq 0.25$. It is assumed that the primary (nanoscale) particles contained in the aggregated structure of the silica particle, effectively serve as asperities, hence explaining the thinning behaviour of silica suspensions in Fig. 3b. It is postulated that although a solvation layer should also exist around the silica particles, their more pronounced surface asperities compared to the relatively smooth glass spheres allows them to penetrate this layer, inducing a reduction in the pressure dependent friction coefficient.

The shear thinning flow curves obtained for the silica suspensions in glycerol can be described well by the Carreau model (eq. 3) for 0.25≤ φ ≤0.34. The estimated parameters (relaxation time, λ and flow index, n) are summarised in Table 2. In order to apply the theory described by Lobry et al. (2019) to our data, the critical stress (τ_c) required for frictional contacts to occur needs to be estimated. To this end, we equate the $\lambda\dot{\gamma}$ term in the Carreau model (Eq. 7) with the ratio of the applied stress to critical stress (i.e. $\lambda\dot{\gamma} = \eta_r\eta_f\dot{\gamma}/\tau_c$), which gives:

$$\tau_c = \frac{\eta_r\eta_f}{\lambda} \tag{7}$$

The suspension relative viscosity (η_r) is taken in the middle of the shear thinning area of the viscosity versus shear rate curve (Fig. 3b), which is more indicative for the λ estimation during fitting, and the corresponding shear rates are also presented in Table 2.

Table 2. Relaxation time (λ) and flow index values (n) as derived from the Carreau fittings in Figure 3b. Relative viscosities (η_r) at the corresponding shear rates ($\dot{\gamma}$) for the estimation of the critical stress values (τ_c), critical load (L_c) and average surface roughness (h_r).

φ	**0.25**	**0.28**	**0.30**	**0.32**	**0.34**
$\boldsymbol{\lambda}$ **(s)**	34.2	225.8	202.2	640.7	677.5
$\boldsymbol{n}$	0.72	0.43	0.35	0.38	0.35
$\boldsymbol{\eta_r}$	6.4	34.7	37.4	115.2	129.0
$\dot{\boldsymbol{\gamma}}$ **(s^{-1})**	0.2	0.025	0.1	0.03	0.08
$\boldsymbol{\tau_c}$ **(Pa)**	0.24	0.20	0.24	0.23	0.25
$\boldsymbol{L_c}$ **(nN)**	0.16 ($\boldsymbol{\tau_{c,average}}$=0.23±0.02 Pa)				
$\boldsymbol{h_r}$ **(μm)**	0.81				

Interestingly, the estimated critical stress values (Table 2) appear to be independent of particle volume fraction, in agreement with the findings of Lobry et al. (2019). The critical stress values enable us to estimate the critical load ($L_c = \tau_c 6\pi\alpha^2$) above which frictional contacts occur leading to shear thinning rheology. The estimated critical load (L_c) is found equal to 0.16 nN (Table 3), which is almost two orders of magnitude lower than the one found by Lobry et al. (2019). The low critical normal load estimated for the silicas can be attributed to the roughness of the particles that facilitates contacts between neighbouring particles at lower loads compared to the relatively smooth particles with very few asperities studied by Lobry et al. (2019). The critical load can be further utilised to obtain an indication of the average particle surface roughness (h_r) following the approach described in Appendix B. A roughness ratio ($= \% h_r/\alpha$) of 13% was estimated, which could explain the high relative viscosities measured for the silica particles in both solvents (Figs. 3 & 4); these are higher than those reported by Tanner and Dai (2016) for a surface roughness of 5%.

3.2 Suspension rheology in mineral oil-adhesion induced shear thinning

Flow curves of all particle suspensions in mineral oil are shown in Figure 4. These suspensions exhibit higher viscosity values compared to the corresponding suspensions in glycerol and a typical yield stress behaviour, while the onset of non-Newtonian response (shear thinning) occurs at concentrations as low as 2% v/v, which are much lower than the ones observed for the suspensions in glycerol.

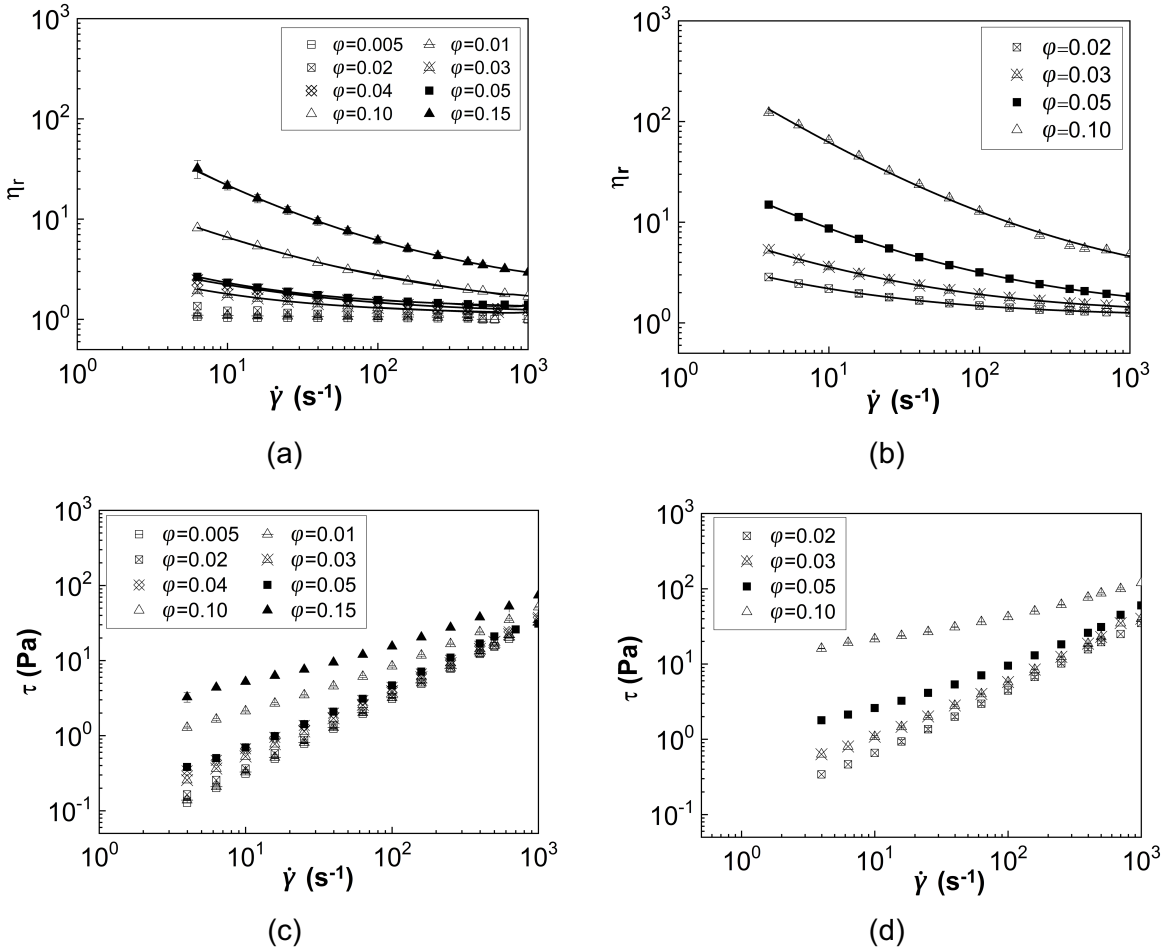

Figure 4. Steady state shear relative viscosity and shear stress of a), c) glass sphere and b), d) silica particle suspensions in mineral oil at 20°C as a function of shear rate. Solid lines correspond to the Herschel-Bulkley fittings. Data below the critical stress for particle sedimentation due to particle solvent density mismatch are excluded.

Mineral oil is non-polar; it consists of a mixture of alkanes and thus, no interactions with the free silanol groups on the silica particle surface are expected. Instead, large particle agglomerates and a gel network are likely to form, giving rise to the flow curves in Figure 4, which are characterised by pronounced shear thinning even at low particle concentrations (Chen et al., 2005; Nicodemo et al., 1974; Selimovic et al., 2007). An asymptotic Newtonian plateau at sufficiently high shear rates ($\dot{\gamma} \geq$500 s^{-1}) can be seen in Fig.4 indicating agglomerate disaggregation under these extreme shear conditions.

The yield stress behaviour of these adhesive particle suspensions is well captured by the Herschel-Bulkley model (eq.4). Fitting the experimental data shown in Figs. 4a and b with eq. 4 yields the infinite shear rate viscosity ($\eta_{r,\infty}$), the yield stress (τ_y) and the relaxation time (λ) values, summarized in Tables 3 and 4 for the glass spheres and silica particle suspensions respectively. The flow index (n) was found equal to 0.5 for all particle concentrations. The yield stress values (τ_y) for both suspensions in mineral oil are presented in Figure 5 as a function of particle volume fraction and a power law relation between τ_y and φ can be observed. The yield stress of the glass sphere suspensions is found to scale as $\tau_y \sim \varphi^3$, in agreement with Snabre and Mills (1996), who reported an exponent of 3 in the presence of rigid agglomerates. On the contrary, the yield stress

for the silica suspensions in mineral oil scales with φ^4, implying a stronger effect of the volume fraction on suspension rheology compared, for example, to colloidal particle dispersions in which the yield stress scales with φ^2 (Eberle et al., 2014; Min Kim et al., 2014). This can be attributed to the fact that the silica particles in our experiments comprise clusters of colloidal particles which should have greater (fractal) surface area, thereby featuring a stronger dependence on volume fraction. It should be noted that the lowest concentration showing yield stress behaviour (φ=0.03) in the glass sphere suspensions does not follow the power law, most likely due to the agglomerates being much smaller at such low particle volume fraction compared to the agglomerates formed at higher concentrations.

Table 3: Relaxation times (λ), infinite shear rate relative viscosity ($\eta_{r,\infty}$) and yield stress values (τ_y) for the glass spheres suspensions in mineral oil as derived from fitting eq. 4 to the experimental data in Fig. 4a.

φ	**0.03**	**0.04**	**0.05**	**0.10**	**0.15**
$\boldsymbol{\lambda\ (s)}$	2.63	6.4	1.29	1.10	0.14
$\boldsymbol{\eta_{r,\infty}}$	1.11	1.15	1.28	1.29	1.77
$\boldsymbol{\tau_y\ (Pa)}$	0.06	0.04	0.07	0.37	2.74

Table 4: : Relaxation times (λ), infinite shear rate relative viscosity ($\eta_{r,\infty}$) and yield stress values (τ_y) for the silica suspensions in mineral oil as derived from fitting eq. 4 to the experimental data in Fig. 4b.

φ	**0.02**	**0.03**	**0.05**	**0.10**
$\boldsymbol{\lambda\ (s)}$	44.47	8.86	0.71	0.03
$\boldsymbol{\eta_{r,\infty}}$	1.16	1.22	1.26	1.99
$\boldsymbol{\tau_y\ (Pa)}$	0.01	0.07	0.61	11.41

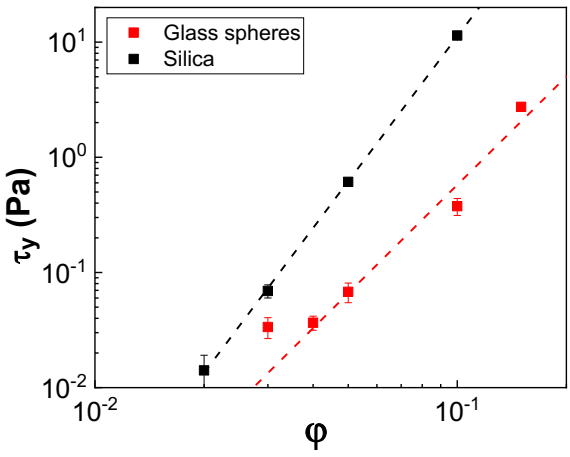

Figure 5. Yield stress values for suspensions in mineral oil at 20°C as a function of particle volume fraction. Dashed lines represent the power law fitting.

Due to the weak interaction of the particles used with mineral oil, as mentioned above, it is reasonable to expect that shear thinning stems from an adhesion driven mechanism, whereby particles form agglomerates at low shear rates, which break down at increasing applied deformations leading to a reduction in suspension viscosity and thus, shear thinning – this will also be reinforced by the optical shearing experiments described below. We can use dimensional analysis arguments and postulate that the adhesion forces (F) for the two types of particles studied, will relate to the yield stress as $\tau_y \sim (F/a^2)\varphi^n$, where α corresponds to the single particle radius and not that of the agglomerates. The resulting estimated adhesion force for the glass spheres is found equal to 0.03 μN, while for the silicas 7 μN. The higher F values estimated for the silica particles are to be expected on the basis of a higher specific surface area, which enhances interparticle interactions in the non-polar solvent. A recent study by our group (Gillissen et al. 2020) showed that a proxy for the adhesion force (F') between particles in adhesive suspensions can be estimated from the asymptotic approach of the suspension viscosity in the limit of infinite shear rate, where particle agglomerates are supposed to have completely broken down. It was found that the silica particles in the present study showed 10 times higher F' values compared to the smooth spheres, highlighting the importance of particle surface morphology to the interparticle interactions even under extreme shear rate conditions (Gillissen et al., 2020).

3.3 Particle volume fraction and infinite shear rheology

To further compare the two suspension systems studied, the infinite shear rate relative viscosity ($\eta_{r,\infty}$), is plotted as a function of the normalised particle volume fraction (φ/φ_m) in Fig. 6. The $\eta_{r,\infty}$ values were derived from fitting eqs. 3 and 4 to the viscosity data of the suspensions in glycerol and in mineral oil respectively. Dotted lines in Fig. 6 represent the Krieger-Dougherty fits (eq. 5) to the experimental data, while grey points refer to data taken from literature. Good agreement between literature and the present results for glass sphere suspensions is observed in both solvents (Fig. 6a, b). The silica particles in glycerol exhibit up to three times higher viscosities compared to the glass spheres at the same volume fractions, especially for $\varphi \geq 0.25$; this is not surprising as the shape irregularity and roughness of the silica particles is expected to increase friction between the particles and hence, energy dissipation (Genovese, 2012; Moon et al., 2015). The latter is in agreement with the study by Tanner and Dai (2016) who reported a 1.5 times increase in viscosity values for a surface roughness of 5% at intermediate shear rates ($\dot{\gamma} = 10\ s^{-1}$), whereas negligible differences between smooth and rough particles were observed at high shear rates ($\dot{\gamma} = 100\ s^{-1}$), in contrast to the rheology of the silica suspensions presented in Fig. 6.

The data presented in Fig. 6b highlight that both particle surface morphology and the physical properties of the suspending medium play a key role in suspension rheology. The suspensions in mineral oil show higher relative viscosities compared to the ones in glycerol, while the degree of viscosity rise in the presence of roughness is even more pronounced at similar φ values. It should be noted that, in mineral oil the maximum concentration for the particles to be sufficiently well dispersed in the solvent was φ=0.15, unlike the suspensions in glycerol, where a maximum φ of

0.62 was achieved. Although suspending the particles in mineral oil limited the range of φ values to achieve a homogeneous suspension, the onset of non-Newtonian rheological behaviour (shear thinning) was shifted to much lower φ compared to suspensions in glycerol. This allowed insights into adhesive system behaviour to be drawn.

The estimated Krieger-Dougherty parameters, summarised in Table 5, provide further comparisons between the particle suspensions studied. Silicas show two times higher intrinsic viscosities (B) and a decrease in the maximum packing fraction (φ_m) compared to the glass sphere suspensions both in glycerol and in mineral oil. Also, suspensions in mineral oil exhibit significantly higher B values and lower φ_m compared to the glycerol case, implying that different mechanisms drive the rheology of the suspensions in the two solvents. More specifically, as also noted above, glycerol is a polar solvent, whose hydroxyl (i.e., -OH) groups are expected to interact with the inherently hydrophilic silicas and hence, minimising the extent of interparticle interactions through the formation of a solvation layer. In contrast, mineral oil is a non-polar solvent and thus, no interaction with the particles is expected to occur. Therefore, particles are allowed to interact with each other forming large agglomerates, which are most likely responsible for increasing the relative viscosity values and decreasing the dispersion capacity and maximum packing fraction of the particles in this solvent.

The data in Fig. 6 were also fitted with an empirical model referring to polydisperse systems (Servais et al., 2002) and the widely used Quemada equation (Quemada, 1978), to account for the polydispersity and surface irregularity of the particles in this study. The formulae of these models and the corresponding estimated parameters, such as the maximum packing fraction, φ_m, are presented and discussed in Appendix A.

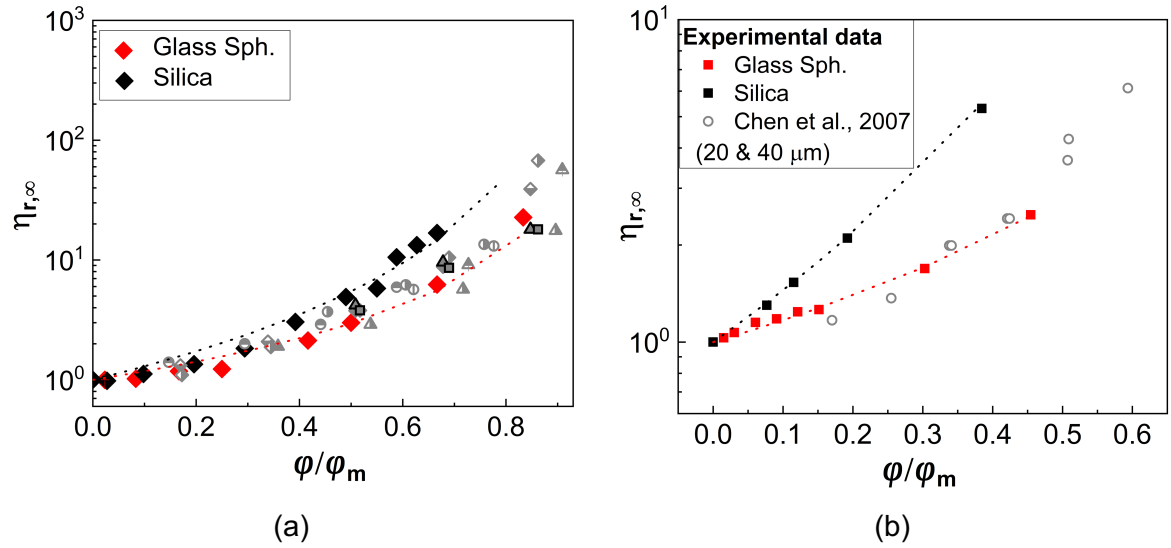

Figure 6. Infinite shear rate relative viscosity values ($\eta_{r,\infty}$) as a function of normalised particle volume fraction (φ/φ_m) for the glass sphere (red points) and silica particle (black points) suspensions in glycerol (a) and in mineral oil (b). Dotted lines represent the Krieger-Dougherty fittings to the experimental results. Comparison between experiments and literature data (grey points) is also shown for both cases. The relevant data reported in literature for frictional suspensions with varying friction coefficients (μ) in (a) are as follows, ◆: Mari et. all ($\mu = 1$) (2014), ▲: Cheal and Ness ($\mu = 0.5$) (2018), ◈: Tanner and Dai (5.3% roughness ratio) (2016) and non-frictional suspensions, ◭: Guy et al. (2015), ◑: Mari et al. (2014), ◓: Gallier et al. (2014), ■: Tanner and Dai (smooth) (2016), ◍: Cheal and Ness ($\mu = 0$) (2018).The scale of the x-axis in a) & b) is different to accommodate better presentation of the results in the two solvents; in mineral oil particle agglomeration narrowed the volume fraction range and thus, φ values only up to 0.15 could be achieved.

Table 5. Intrinsic viscosity (B) and maximum packing fraction (φ_m) for the suspensions in glycerol and in mineral oil as derived from the Krieger-Dougherty fittings in Figure 6.

Sample	**Glycerol**		**Mineral oil**	
	B	φ_m	B	φ_m
Glass Spheres	2.60	0.60	4.5	0.33
Silicas	4.80	0.51	13.3	0.26

3.4 Suspension microstructure: optical shearing

To further elucidate the frictional and adhesive particle interactions and their role in the observed shear thinning behaviour, the suspension microstructure was visualised by means of an optical shearing method (Fig. 2), also allowing us to quantify the agglomeration and dispersion characteristics of the sheared suspensions *in situ*. Figures 7 and 8 present sample images for glass sphere and silica suspensions in glycerol and in mineral oil respectively at low ($\dot{\gamma}$=1 s^{-1}), medium ($\dot{\gamma}$=10 s^{-1}) and high ($\dot{\gamma}$=100 s^{-1}) shear rates. Optical methods are limited by the opacity of the sample and thus, visualisation of suspension microstructure could only be achieved under relatively dilute conditions; hence suspensions of 5% and 3% v/v were used. The microstructure of the suspensions in glycerol (Fig. 7) shows no apparent dependence either on the shear rate or

the type of particles, which also agrees with the Newtonian behaviour of these suspensions under steady state shear, as shown in Figure 3.

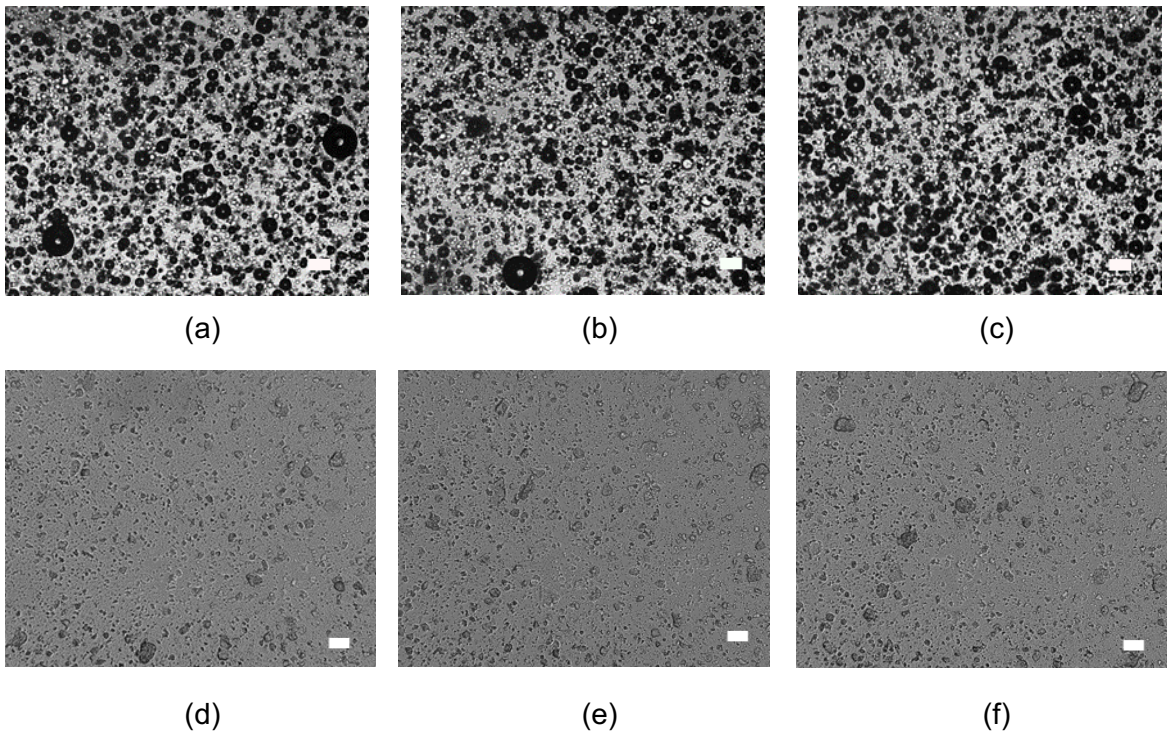

Figure 7. Microstructure data obtained for 5% v/v glass sphere (top) and 3% v/v silica (bottom) suspensions in glycerol at shear rates: 1 s^{-1} (a, d); 10 s^{-1} (b, e) & 100 s^{-1} (c, f). The scale bars (▬) correspond to 40 μm length.

On the contrary, both the shear rate and particle surface properties significantly affect the microstructure of particle suspensions in mineral oil (Fig. 8). More specifically, at $\dot{\gamma}$=1 s^{-1} glass spheres form large randomly shaped agglomerates (Fig. 8a), while silica particles agglomerate forming large elongated clusters which extend to the whole image (Fig. 8d). These structures can explain the differences in the estimated values of the adhesion forces between the glass spheres and the silica particles. When the shear is increased by one order of magnitude ($\dot{\gamma}$=1 s^{-1} to 10 s^{-1}), particle agglomerates start to break down and reduce in size (Figs. 8b & e); this helps explain the observed shear thinning behaviour of the suspensions in mineral oil under steady state shear, as depicted in Figure 4. At the relatively high shear rates ($\dot{\gamma}$=100 s^{-1}) agglomerates seem to have completely broken to single units and the whole image area is covered with particles (Figs.8c & f).

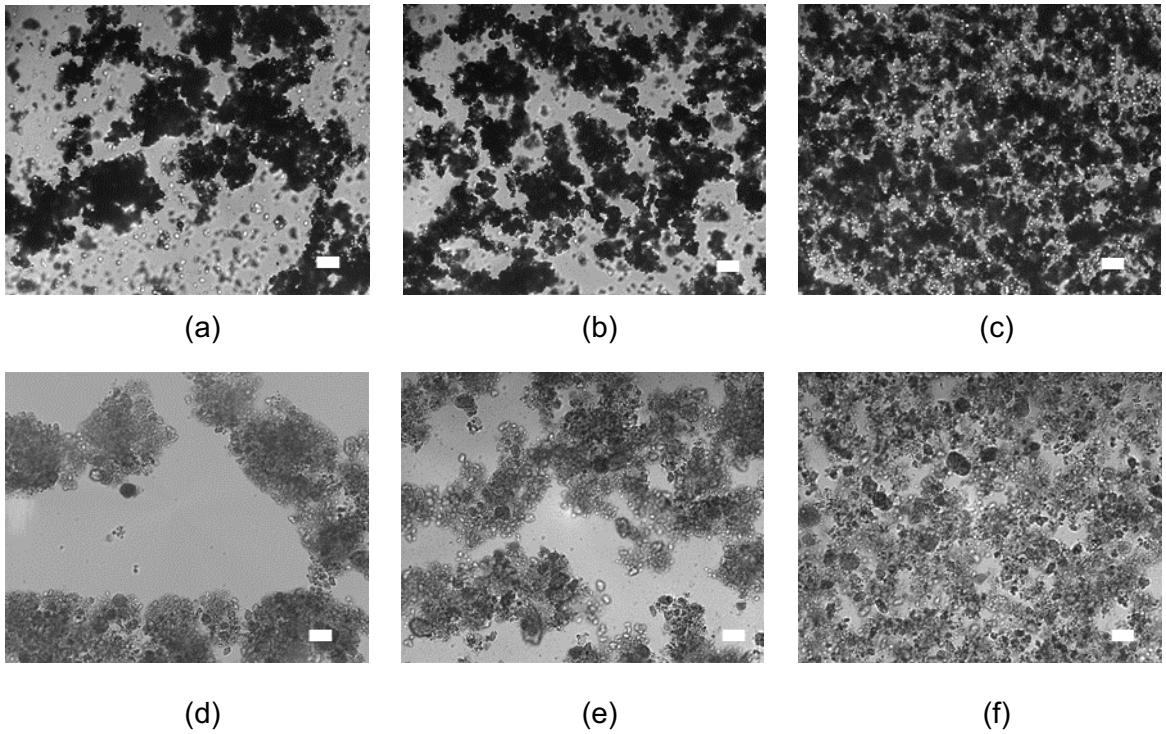

Figure 8. Microstructure data obtained for 5% v/v glass sphere (top) and 3% v/v silica (bottom) suspensions in mineral oil at shear rates: 1 s^{-1} (a, d); 10 s^{-1} (b, e) & 100 s^{-1} (c, f). The scale bars (▬) correspond to 40 μm length.

In order to quantify suspension microstructure and to characterise the extent of particle agglomeration, sets of 2000 images were obtained at different shear rates and analysed in MATLAB. The acquired images were first binarized by applying a local threshold to account for the range of image intensities and distinguish between particles and fluid areas in the image, especially in the case of silicas. The areas free of particles, turned to white, were labelled and then measured by applying the *regionprops* function in MATLAB. The measured areas were used in conjunction with eq. 6 to calculate the aggregation index, A. The estimated A values, are normalised with the index value obtained at the highest shear rate employed in each case to facilitate the comparison. The normalised aggregation indices (A_N) are plotted in Figure 9 for the 5% v/v glass spheres (a) and 3% v/v silica particles (b) in mineral oil and in glycerol. The A_N for the non-adhesive glycerol suspensions remain constant and close to one since no microstructure changes occurred in the low concentrations imaged; they are also shown in Fig. 9 for reference. In contrast, suspensions in mineral oil exhibit a progressive decrease of the aggregation index with shear rate and this trend is also reflected in the corresponding relative viscosity curve – shown as inset figures for the same range of shear rates – especially for the silica particles. The latter further confirms that the shear thinning behaviour of these suspensions is driven by adhesion between the particles.

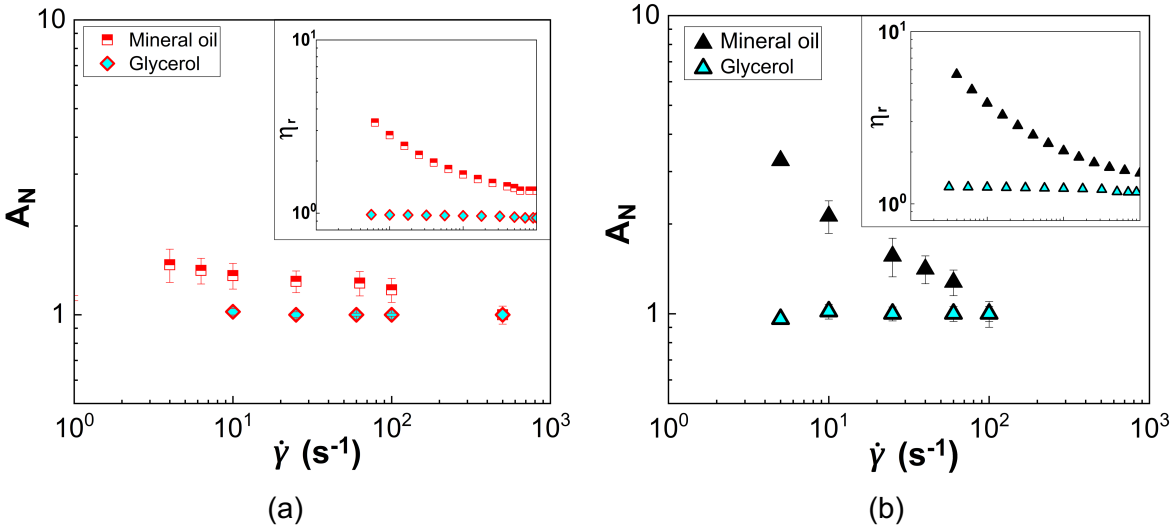

Figure 9. Normalised aggregation index for selected suspensions in glycerol and in mineral oil for a) a 5% v/v glass spheres and b) a 3% v/v silica suspension as a function of shear rate. The insets represent the relative viscosity values vs shear rate for the corresponding suspensions in both solvents.

3.5 Validation: Tuning particle interactions to control shear thinning

The previous sections highlighted the role of interparticle interactions on suspension rheology and in particular, the mechanisms leading to shear thinning behaviour. The latter is desirable in many industrial applications; the ability to predict and control interparticle interactions can enable designing formulations with required rheological properties, optimising thus, manufacturing processes. Modifying particle surface chemistry provides such a tuning mechanism and it can also be exploited to enhance the particle dispersion capacity in different solvents (Hayashi and Kawaguchi, 2017; Işçi et al., 2007; Marunaka and Kawaguchi, 2017, 2014; Zhang et al., 2017). Better dispersion also means that particle functionalisation can help tune the maximum packing fraction (Hayashi and Kawaguchi, 2017).

In the present work, we use particle surface functionalisation to improve the dispersion of particles in solvents and enable particle-solvent interactions to dominate over the particle-particle adhesive forces; providing a route to altering the shear thinning mechanism of suspensions. More specifically, the glass sphere surface chemistry was modified with the addition of hydrophobic groups to improve their dispersion in mineral oil. Glass spheres were treated with two agents, i.e. palmitic acid and perfluorooctyltriethoxysilane, which are known to bind on the free silanol groups of glass spheres, weakening interparticle interactions (Chen et al., 2005; Go et al., 2017; Song et al., 2014; Yao Lu et al., 2015). The bonding mechanisms for the two agents are illustrated in Figure 10. The fluorosilane forms a siloxane bond between its silicon element and the free oxygens on the silica surface. On the other hand, in the case of palmitic acid an ester bond is created between its carboxyl group and the free silanol groups on silicas. These two molecules have chain lengths that are three orders of magnitude smaller than the particle average diameter and thus, they are not expected to affect particle original diameter.

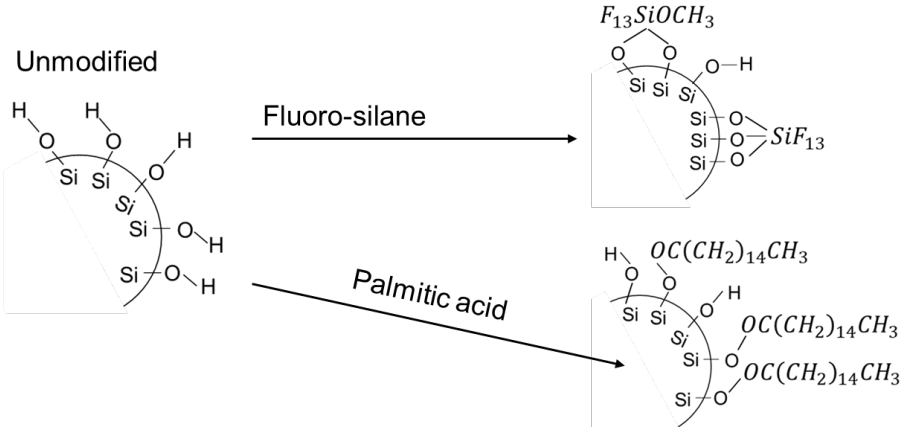

Figure 10: Schematic representation of the glass sphere surface chemistry modification. In the case of fluorosilane, a siloxane bond is created between the free hydroxyl group on silica and the silicon, whereas in the palmitic acid case, an ester bond is created between the hydroxyl group on silica and the carboxylic end of the reagent.

Figure 11a compares the relative viscosity values versus shear rate for a 5% v/v suspension of untreated and treated glass spheres in mineral oil, while Figure 11b presents the corresponding yield stress values and equivalent adhesion forces for the same suspensions. Two different concentrations of palmitic acid (Palm.Acid36 and Palm.Acid60) with differing amounts of hydrophobic groups were employed. The adhesion forces for the treated particle suspensions were estimated using the relation $\tau_y \propto (F/a^2)\varphi^n$ where n was taken equal to 3, as found from the rheology of the untreated particles. As the concentration of the palmitic acid increases, the viscosity and yield stress values of the suspensions significantly decrease, which indicates a reduction in interparticle interactions as well as a better affinity between the particles and the mineral oil. Interestingly, at relatively high shear rates, all suspensions of treated glass spheres reach an asymptotic Newtonian plateau with a relative viscosity close to unity (i.e. $\eta_s = \eta_{fMO}$), while the untreated particles show higher relative viscosity values. The behaviour of the former implies that treated particles form weaker agglomerates compared to the untreated case, which completely disaggregate to individual units at $\dot{\gamma}$>100 s^{-1} and can no longer affect solvent viscosity at such low concentrations, as observed in the glycerol case. The adhesion forces decrease proportionally to the yield stress, as shown in Fig. 11b. Therefore, controlling interparticle interactions through the particle surface chemistry introduces new insights in suspension rheology and can be exploited to tune rheology and enable the manufacturing of complex formulations.

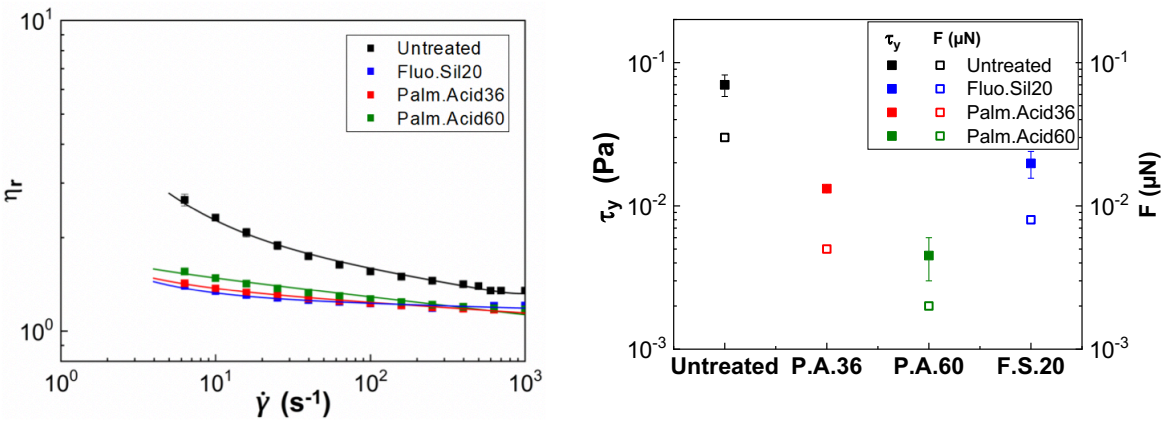

Figure 11. a) Relative viscosity values (η_r) as a function of shear rate for selected untreated and treated glass spheres in mineral oil at a concentration of 5% v/v and 20°C. b) Yield stress (τ_y) and equivalent adhesion force (F) for the treated and untreated glass sphere suspensions shown in (a). The numbers in the legend next to the hydrophobic agents represent the % w/w concentration of the reagent in relation to particle mass.

Figure 12 shows sample images of the untreated glass spheres (Fig.12a) and the glass spheres treated with fluorosilane (Fig.12b) in mineral oil and at a low concentration of $\varphi = 0.01$ so that the size of single elements can be measured. These images were taken in the absence of shearing, following the preparation of the samples through high shear mixing. The acquired images were analysed in MATLAB and the maximum particle equivalent diameter was estimated for each case indicating a clear reduction in the particle agglomerate size when the particle surface chemistry was altered with the introduction of the hydrophobic groups. The d_{95}, i.e. the particle diameter at which 95% of the measured particles have a size below this number, of the untreated glass spheres in water is also included in Fig. 12 for comparison. The latter further confirms that particle attraction was hindered through particle surface chemistry functionalisation.

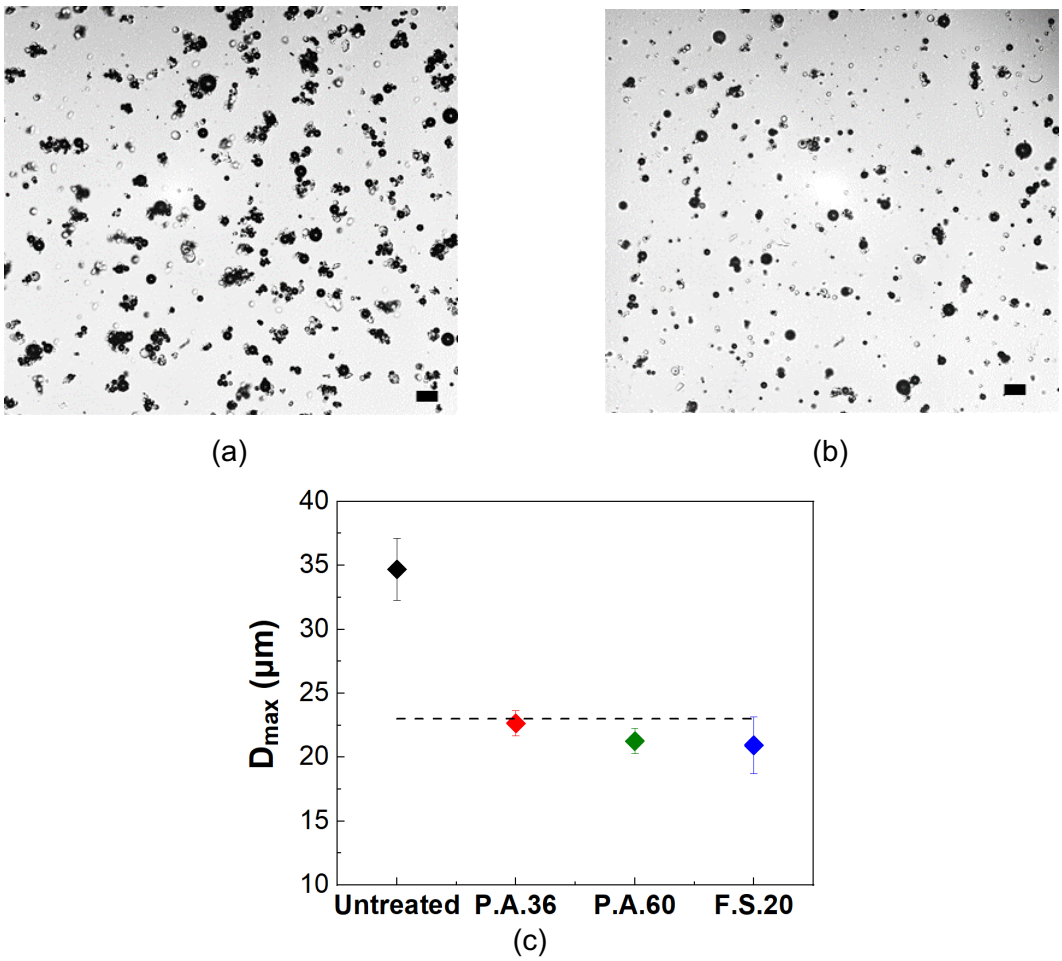

Figure 12: Indicative sample images of the untreated glass spheres (a) and glass spheres treated with fluorosilane (b) in mineral oil at $\varphi = 0.01$ under static conditions. The scale bars (▬) correspond to a length of 40 µm; c) Comparison of the maximum diameter for each suspension between the treated and untreated particles as observed under the microscope. The dashed line represents the d_{95} of the untreated glass sphere suspension in water. i.e. the diameter at which 95% of the measured particles have a size below this number.

3.6 Extent of shear thinning behaviour and effect of critical stresses

The extent of shear thinning ($\eta_{r,e}$) as a function of particle volume fraction is summarised in Figure 13a for all the suspensions investigated in the present study. $\eta_{r,e}$ is defined as the ratio between the difference of the low shear relative viscosity ($\eta_{r,6}$, taken at $\dot{\gamma}$=6.3 s^{-1} for all the shear thinning suspensions in glycerol and in mineral oil to avoid sedimentation effects) and infinite shear relative viscosity to the infinite shear rate relative viscosity ($\eta_{r,\infty}$) values, as derived from eq. 3 and 4 (i.e. $(\eta_{r,6} - \eta_{r,\infty})/\eta_{r,\infty}$). More specifically, the suspensions in glycerol show shear thinning behaviour at concentrations higher than 25% due to frictional contacts between neighbouring particles at sufficiently high normal loads. On the other hand, suspensions in mineral oil start to shear thin at much lower concentrations (φ=0.02) compared to the glycerol case, due to the formation and disaggregation of particle agglomerates. Moreover, by adding hydrophobic groups on the surface of the inherently hydrophilic glass spheres, we managed to suppress the shear thinning response as shown from the reduction in the $\eta_{r,e}$ values.

The critical stresses for the silica suspensions in glycerol responsible for the onset of shear thinning and the yield stress values for both suspensions in mineral oil are also presented as a function of φ in Fig. 13b. Suspensions in glycerol show a φ-independent critical stress, in agreement with the frictional model described by Lobry et al. (2019), while adhesive particle suspensions exhibit typical yield stress behaviour that highly depends on particle volume fraction.

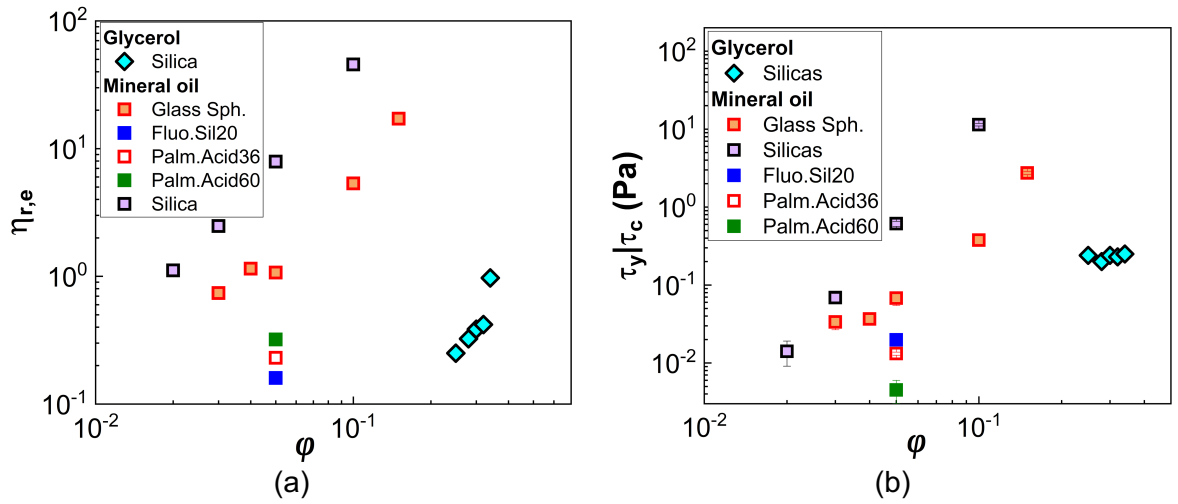

Figure 13. Summary of a) the extent of shear thinning as a function of particle volume fraction for all the non-Newtonian (shear thinning) suspensions; b) the estimated critical stresses (τ_c), giving rise to shear thinning, for the silica suspensions in glycerol and the yield stress (τ_y) values for both suspensions in mineral oil.

4. Conclusions

In the present work, we examined the rheological properties of non-Brownian polydisperse glass spheres and commercial silica particles over a range of shear rates and particle volume fractions. By utilising particle surface morphology and the solvents' physical properties we evidenced two distinct mechanisms for the shear thinning response of such suspensions. In glycerol, where strong interactions between the solvent and the particles occur, smooth glass spheres showed no shear thinning even at high volume fractions (φ≥0.5), while rough silica particles, with similar size distribution, induced shear thinning behaviour at φ≥0.25. The latter was explained in the light of a friction driven mechanism induced by surface roughness at sufficiently high normal loads. Considering surface irregularity as elastically deformable asperities, we were able to estimate the critical load above which two neighbouring rough particles experience frictional contacts. At increasing applied pressure (load), the shear strength between the particles decreases leading to a reduced friction coefficient and shear thinning response.

The second mechanism to induce shear thinning was based on the adhesive forces between particles when suspended in a non-polar solvent. In mineral oil, the solvent-particle interactions are weak and thus, interparticle interactions (adhesion) are expected to dominate the suspensions rheology. The suspensions in mineral oil showed pronounced shear thinning and yield stress behaviour at concentrations as low as 2% v/v for both glass spheres and rough silicas. This was

attributed to the particles forming large agglomerates at low shear rates, which break down at increasing applied deformations leading to shear thinning. Particle agglomeration and disaggregation was reinforced by means of an optical shearing method, which enabled us to actually visualise and further quantify aggregation characteristics through estimating an aggregation index.

Finally, the generality of our findings was established through modifying the surface chemistry of the glass spheres by introducing hydrophobic groups. Two different self-assembled monolayers, i.e. palmitic acid and fluorosilane, with varying concentrations of hydrophobic groups were employed. This treatment inhibited interparticle interactions between the inherently hydrophilic glass spheres in mineral oil, as demonstrated by a decrease in the yield stress and adhesion force values, leading to reduced shear thinning behaviour. The results clearly elucidate the importance of being able to predict and control interparticle interactions and provide a framework for silica suspension rheology. The latter can serve as a significant tool for the design and optimisation of formulations with required rheological properties tailored to specific applications.

Acknowledgements

The authors would like to thank their industrial collaborators Dr Robert Sochon, Mark Jackson and Dr Andrew Johnson from GlaxoSmithKline Plc for the contribution of silica particles and useful discussions. Also, Dr Yao Lu and Dr Vikramjeet Singh for useful discussions and advice during particle surface modification. The particle size distributions were conducted by Keith Sanderson from Microtrac. This work was funded by the EPSRC grant on Future Formulations (EP/N024915/1) and UCL Mechanical Engineering.

APPENDIX A

The relative viscosity data as a function of particle volume fraction (Fig. 3) were fitted with two more empirical equations to account for particle polydispersity and surface irregularities (Quemada, 1978; Servais et al., 2002); parameters that better reflect the properties of the particle involved in this study.

$$\eta_r = \left[1 + \left(\frac{b\varphi}{1 - {}^{\varphi}/_{\varphi_m}}\right)\right]^{3.3\varphi_m} \quad \text{(A.1)}$$

$$\eta_r = \left(1 - \frac{\varphi}{\varphi_m}\right)^{-2} \quad \text{(A.2)}$$

, where φ_m is the maximum packing fraction and b is an adjustable parameter accounting for particle polydispersity.

The estimated parameters derived from fitting equations A.1 and A.2 to the experimental data presented in Fig. 3 are summarized in Table A1. The maximum packing fraction estimated using

the equation for polydisperse systems (eq. A.1) was the same with that derived from the Krieger-Dougherty equation for the glass sphere suspensions in glycerol, while the corresponding φ_m value for the silica suspensions was 16% lower. Remarkably, the Quemada model yielded the closest to the theory results for both particle suspensions in glycerol as described for polydisperse randomly closed packed spheres (φ_m≥0.64) and rough crystals (φ_m=0.44) (Genovese, 2012). Suspensions in mineral oil showed lower maximum packing fractions for both particle types in accordance to the Krieger-Dougherty results. Moreover, silica suspensions showed higher b values compared to glass spheres in glycerol and the same trend was also observed for the glass spheres suspensions in mineral oil, reflecting a broader size distribution due to particle agglomeration. In general, deviations of the obtained maximum packing fractions (φ_m) from the theory but also between the different fitted equations might occur due to the polydispersity and surface irregularity of the particles used in this study; parameters not accounted in all the existing empirical models. For example, the Krieger-Dougherty model was built upon semi-dilute suspensions of perfectly spherical and monodisperse particles. Also, the degrees of freedom (i.e. number of estimated variables) included in the different equations might affect the values derived during the fitting process. The Quemada model has only one degree of freedom (i.e. maximum packing fraction), which might ease the fitting of this model to the data.

Table A1: Summary of the estimated parameters (i.e. maximum packing fraction, φ_m , and b) derived by fitting eq. A.1 and A.2 to the experimental data in Fig. 3.

Estimated parameters / Suspending media	**Servais et al. (2002)**		**Quemada (1978)**
	$\boldsymbol{\varphi_m}$	$\boldsymbol{b}$	$\boldsymbol{\varphi_m}$
Glass spheres			
Glycerol	0.60	1.24	0.68
Mineral oil	0.27	5.25	0.41
Silicas			
Glycerol	0.43	3.65	0.44
Mineral oil	N/A	N/A	0.18

APPENDIX B

The approach used to estimate the average surface roughness of the silica particles is presented below. The equations used were taken from Lobry et al. 2019.

$$\overline{L_c} = [8.88\nu - 10.13(\nu^2 + 0.089)] \quad \text{(B.1)}$$

$$C_\nu = 1.234 + 1.256\nu \quad \text{(B.2)}$$

$$L_c = \overline{L_c}\pi^3 \frac{Y_o}{6} {C_\nu}^3 \left(h_r \frac{2(1-\nu^2)}{E} Y_0\right)^2 \quad \text{(B.3)}$$

Combining the three equations above, a relation for the particle surface roughness can be obtained.

$$h_r = \frac{E\sqrt{{L_c}/{\overline{L_c}}\pi^3\frac{Y_o}{6}{C_v}^3}}{2(1-\nu^2)Y_0} \quad \text{(B.4)}$$

Table B1: Mechanical properties of silicas.

Young modulus (E)	66.3 GPa
Yield strength (Y_0)	45 MPa
Poisson's ratio (ν)	0.15

References

Amiri, A., Øye, G., Sjöblom, J., 2012. Stability and Flow-Induced Flocculation of Fumed Silica Suspensions in Mixture of Water-Glycerol. J. Dispers. Sci. Technol. 338, 1247–1256.

Archard, J.F., 1957. Elastic deformation and the laws of friction. Proc. R. Soc. Lond. A 243, 190–205.

Blanc, F., D'Ambrosio, E., Lobry, L., Peters, F., Lemaire, E., 2018. Universal scaling law in frictional non-Brownian suspensions. Phys. Rev. Fluids 3, 114303-1–12.

Boyd, J., Buick, J.M., Green, S., 2007. Analysis of the Casson and Carreau-Yasuda non-Newtonian blood models in steady and oscillatory flows using the lattice Boltzmann method. Phys. Fluids 19, 093103-1–14.

Chatté, G., Comtet, J., Niguès, A., Bocquet, L., Siria, A., Ducouret, G., Lequeux, F., Lenoir, N., Ovarlez, G., Colin, A., 2018. Shear thinning in non-Brownian suspensions. Soft Matter 14, 865–1070.

Chen, S., Øye, G., Sjöblom, J., 2005. Rheological properties of silica particle suspensions in mineral oil. J. Dispers. Sci. Technol. 26, 791–798.

De Kruif, C.G., Van Iersel, E.M.F., Vrij, A., Russel, W.B., 1985. Hard sphere colloidal dispersions: Viscosity as a function of shear rate and volume fraction. J. Chem. Phys. 83, 4717–4725.

Dinkgreve, M., Paredes, J., Denn, M.M., Bonn, D., 2016. On different ways of measuring "the" yield stress. J. Nonnewton. Fluid Mech. 238, 233–241.

Eberle, A.R., Martys, N., Porcar, L., Kline, S.R., George, W.L., Kim, J.M., Butler, P.D., Wagner, N.J., 2014. Shear viscosity and structural scalings in model adhesive hard-sphere gels. Phys. Rev. E 89, 050302-(1-5).

Egres, R.G., Nettesheim, F., Wagner, N.J., 2006. Rheo-SANS investigation of acicular-

precipitated calcium carbonate colloidal suspensions through the shear thickening transition. J. Rheol. 50, 685–709. https://doi.org/10.1122/1.2213245

Foss, D.R., Brady, J.F., 2000. Structure, diffusion and rheology of Brownian suspensions by Stokesian Dynamics simulation. J. Fluid Mech 407, 167–200.

Gadala-Maria, F., Acrivos, A., 1980. Shear-induced structure in a concentrated suspension of solid spheres. J. Rheol. 24, 799–1693. https://doi.org/10.1122/1.551021

Galindo-Rosales, F.J., Rubio-Hernandez, F.J., 2009. Static and Dynamic Yield Stresses of Aerosil® 200 Suspensions in Polypropylene Glycol. Appl. Rheol. 20, 22787-1–10.

Gallier, S., Lemaire, E., Peters, F., Lobry, L., 2014. Rheology of sheared suspensions of rough frictional particles. J. Fluid Mech. 757, 514–549.

Gamonpilas, C., Morris, J.F., Denn, M.M., 2016. Shear and normal stress measurements in non-Brownian monodisperse and bidisperse suspensions. J. Rheol. 60, 289–296.

Gao, J., Mwasame, P.M., Wagner, N.J., 2017. Thermal rheology and microstructure of shear thickening suspensions of silica nanoparticles dispersed in the ionic liquid [C 4 mim][BF 4]. J. Rheol. 61, 525–535.

Genovese, D.B., 2012. Shear rheology of hard-sphere, dispersed, and aggregated suspensions, and filler-matrix composites. Adv. Colloid Interface Sci. 171–172, 1–16.

Gillissen, J.J.J., Papadopoulou, A., Tiwari, M.K., Balabani, S., Wilson, H.J., 2020. Suspension rheology of adhesive particles at high shear-rates. Phys. Rev. Fluids.

Go, M.-R., Bae, S.-H., Kim, H.-J., Yu, J., Choi, S.-J., 2017. Interactions between Food Additive Silica Nanoparticles and Food Matrices. Front. Microbiol. 8, 1–12.

Gunes, D.Z., Scirocco, R., Mewis, J., Vermant, J., 2008. Flow-induced orientation of non-spherical particles: Effect of aspect ratio and medium rheology. J. Nonnewton. Fluid Mech. 155, 39–50.

Hayashi, H., Kawaguchi, M., 2017. Effects of the degree of surface modification on the rheological responses of precipitated silica suspensions in benzyl alcohol. J. Dispers. Sci. Technol. 38, 737–742.

Işçi, S., Güngör, N., Alemdar, A., Isik Ece, Ö., 2007. Influence of clay surface modification on morphology and rheology of polyethylene glycol/montmorillonite nanocomposites. J. Compos. Mater. 41, 1521–1533.

Kaliviotis, E., Dusting, J., Sherwood, J.M., Balabani, S., 2016. Quantifying local characteristics of velocity, aggregation and hematocrit of human erythrocytes in a microchannel flow. Clin. Hemorheol. Microcirc. 63, 123–148.

Kaliviotis, E., Yianneskis, M., 2007. On the effect of dynamic flow conditions on blood microstructure investigated with optical shearing microscopy and rheometry. Proc. Inst. Mech. Eng. Part H J. Eng. Med. 221, 887–897.

Kalman, D.P., Wagner, N.J., 2009. Microstructure of shear-thickening concentrated suspensions determined by flow-USANS. Rheol. Acta 48, 897–908.

Katepalli, H., John, V.T., Tripathi, A., Bose, Arijit, Bose, A, 2017. Microstructure and rheology of particle stabilized emulsions: Effects of particle shape and inter-particle interactions. J. Colloid Interface Sci. 485, 11–17.

Khandavalli, S., Rothstein, J.P., 2015. Large amplitude oscillatory shear rheology of three different shear-thickening particle dispersions. Rheol Acta 54, 601–618.

Krieger, I.M., Dougherty, T.J., 1959. A Mechanism for Non-Newtonian Flow in Suspensions of Rigid Spheres. Trans. Soc. Rheol. 3, 137–152.

Lin, Y.-J., Barman, S., He, P., Zhang, Z., Christopher, G.F., Lisa Biswal, S., 2018. Combined interfacial shear rheology and microstructure visualization of asphaltenes at air-water and oil-water interfaces. J. Rheol. 62, 1-10

Lobry, L., Lemaire, E., Blanc, F., Gallier, S., Peters, F., 2019. Shear thinning in non-Brownian suspensions explained by variable friction between particles. J. Fluid Mech. 860, 682–710.

Ma, A.W.K., Mackley, M.R., Chinesta, F., 2008. The microstructure and rheology of carbon nanotube suspensions. Int. J. Mater. Form. 1, 75–81.

Ma, T., Yang, R., Zheng, Z., Song, Y., 2017. Rheology of fumed silica/polydimethylsiloxane suspensions. J. Rheol. 61, 205–215.

Macosko, C.W., 1994. Rheology: Principles, Measurements and Applications, 1st ed. Wiley-VCH, United States of America.

Maranzano, B.J., Wagner, N.J., 2001. The effects of interparticle interactions and particle size on reversible shear thickening: Hard-sphere colloidal dispersions. J. Rheol. 451, 1205–111.

Marunaka, R., Kawaguchi, M., 2017. Rheological behavior of hydrophobic fumed silica suspensions in aromatic dispersion media. J. Dispers. Sci. Technol. 38, 223–228.

Marunaka, R., Kawaguchi, M., 2014. Rheological behavior of hydrophobic fumed silica suspensions in different alkanes. Colloids Surfaces A Physicochem. Eng. Asp. 456, 75–82.

Massaro, R., Colombo, G., Puyvelde, P. Van, Vermant, J., 2020. Viscoelastic cluster densification in sheared colloidal gels. Soft Matter 16, 2437–2447.

Mewis, J., Wagner, N.J., 2012. Colloidal Suspension Rheology, 1st ed. Cambridge University Press, New York.

Min Kim, J., Eberle, A.P.R., Kate Gurnon, A., Porcar, L., Wagner, N.J., 2014. The microstructure and rheology of a model, thixotropic nanoparticle gel under steady shear and large amplitude oscillatory shear (LAOS). J. Rheol. 58, 1301–1328.

Moon, J.Y., Dai, S., Chang, L., Lee, J.S., Tanner, R.I., 2015. The effect of sphere roughness on the rheology of concentrated suspensions. J. Nonnewton. Fluid Mech. 223, 233–239.

Morris, J.F., 2009. A review of microstructure in concentrated suspensions and its implications for rheology and bulk flow. Rheol. Acta 48, 909–923.

Nicodemo, L., Nicolais, L., Landel, R.F., 1974. Shear rate dependent viscosity of suspensions in newtonian and non-newtonian liquids. Chem. Eng. Sci. 29, 729–735.

Quemada, D., 1978. Rheology of concentrated disperse systems II. A model for non-newtonian shear viscosity in steady flows. Rheol. Acta 17, 632–642.

Raghavan, S.R., Walls, H.J., Khan, S.A., 2000. Rheology of silica dispersions in organic liquids: New evidence for solvation forces dictated by hydrogen bonding. Langmuir 16, 7920–7930.

Saint-Michel, B., Manneville, S., Meeker, S., Ovarlez, G., Bodiguel, H., 2019. X-ray Radiography of Viscous Resuspension. Phys. Fluids 31, 103301-1–17.

Selimovic, S., Maynard, S.M., Hu, Y., 2007. Aging effects of precipitated silica in poly(dimethylsiloxane). J. Rheol. 51, 325–340.

Servais, C., Jones, R., Roberts, I., 2002. The influence of particle size distribution on the processing of food. J. Food Eng. 51, 201–208.

Sierou, A., Brady, J.F., 2002. Rheology and microstructure in concentrated noncolloidal suspensions. J. Rheol. 46, 1031–1056.

Song, J., Huang, S., Lu, Y., Bu, X., Mates, J.E., Ghosh, A., Ganguly, R., Carmalt, C.J., Parkin, I.P., Xu, W., Megaridis, C.M., 2014. Self-Driven One-Step Oil Removal from Oil Spill on Water via Selective-Wettability Steel Mesh. Appl. Mater. interfaces 6, 19858−19865.

Tanner, R.I., 2018. Aspects of non-colloidal suspension rheology. Phys. Fluids 30, 101301(1–13).

Tanner, R.I., 2015. Non-colloidal suspensions: Relations between theory and experiment in shearing flows. J. Nonnewton. Fluid Mech. 222, 18–23.

Varga, Z., Grenard, V., Pecorario, S., Taberlet, N., Dolique, V., Manneville, S., Divoux, T., McKinley, G.H., Swan, J.W., 2019. Hydrodynamics control shear-induced pattern formation in attractive suspensions. Proc. Natl. Acad. Sci. 116, 12193–12198.

Yao Lu, Sanjayan Sathasivam, Jinlong Song, Colin R. Crick, Claire J. Carmalt, Ivan P. Parkin, 2015. Robust self-cleaning surfaces that function when exposed to either air or oil. Repel. Mater. 347, 1132–1135.

Zhang, S., Sha, N., Zhao, Z., 2017. Surface modification of α-Al2O3 with dicarboxylic acids for the preparation of UV-curable ceramic suspensions. J. Eur. Ceram. Soc. 37, 1607–1616.

Zhou, J.Z.Q., Tunan Fang, Guihua Luo, Peter HT Uhlherr, 1995. Yield stress and maximum packing fraction of concentrated suspensions. Rheol. Acta 34, 544–561.